

# Universal quantum computation without state distillation on a 2-D color code

Austin G. Fowler

*Institute for Quantum Computing, University of Waterloo, Waterloo, ON, N2L 3G1, CANADA*

(Dated: March 18, 2019)

Recent work on fault-tolerant quantum computation making use of topological error correction has led to powerful computation schemes that require only local interactions yet permit fast long-range logical gates and error correction with a threshold error rate approaching 1% [1, 2, 3, 4, 5]. One weakness of these schemes is that they make use of state distillation to achieve universal computation, an approach that involves a huge ancilla factory that does nothing more than generate special logical states yet must be several orders of magnitude larger than the rest of the computer to provide these states at a sufficient rate. In this work, we present a new fault-tolerant quantum computation scheme making use of topological error correction on a 2-D color code that possesses all of the desirable features of these recent schemes yet does not require state distillation, thereby reducing the resource requirements by several orders of magnitude.

## I. INTRODUCTION

Classical computers manipulate bits that can be exclusively 0 or 1. Quantum computers manipulate quantum bits (qubits) that can be placed in arbitrary superpositions  $\alpha|0\rangle + \beta|1\rangle$  and entangled with one another to create states such as  $(|00\rangle + |11\rangle)/\sqrt{2}$ . This additional flexibility provides both additional computing power [6, 7, 8, 9, 10, 11] and additional challenges when attempting to cope with the now quantum errors in the computer [12, 13, 14]. An extremely efficient scheme for quantum error correction and fault-tolerant quantum computation is required to correct these errors without making unphysical demands on the underlying hardware and without introducing excessive time overhead and thus wasting a significant amount of the potential performance increase.

Recently, significant progress towards practical quantum error correction and fault-tolerant quantum computation has been made by making use of topological error correction [1, 2, 3, 4, 5]. These schemes feature a single error correcting code used for the entire computer with qubits associated with holes or “defects” deliberately introduced using measurements. Logical qubits can be both initialized and measured in the  $X_L$  and  $Z_L$  bases. Logical CNOT can be performed by braiding defects around one another. In some of these schemes, individual logical qubits can be isolated and some transversal single logical qubit operations applied [3, 4]. All of these recently developed schemes possess a sufficiently broad range of gates to enable state distillation [15, 16] and thus achieve universality, but none possess a sufficiently broad range of gates to enable universal computation without state distillation.

State distillation is typically used to produce a better copy of one or both of the states  $|Y\rangle = (|0\rangle + i|1\rangle)/\sqrt{2}$  and  $|A\rangle = (|0\rangle + e^{i\pi/4}|1\rangle)/\sqrt{2}$  consuming either 7 or 15 imperfect copies of these states, respectively. Given reasonable assumptions about the desired logical error rate and the underlying physical error rate, three or more concatenated layers of state distillation can easily be required

to produce sufficiently high fidelity states [2]. A single Toffoli gate requires 7 accurate copies of  $|A\rangle$  and up to 7 accurate copies of  $|Y\rangle$  [2, 17]. Depending on the details of the quantum algorithm being executed, the ancilla factory required to produce a sufficiently high rate of distilled states can easily be several orders of magnitude larger than the rest of the computer. Eliminating the need for state distillation can thus easily result in a reduction of the required number of qubits by several orders of magnitude.

In this work, we combine a specific 2-D color code [18] with the techniques of defect braiding, defect isolation and transversal rotation to produce a sufficiently broad range of fault-tolerant gates to achieve universality without state distillation. Our scheme calls for a 2-D array of qubits with local tunable interactions and a measurement time of the same order as the gate times. It features a high threshold estimated to lie between  $10^{-3}$  and  $10^{-2}$  given its similarity to the scheme of [1, 2], which has a threshold error rate of approximately  $7.5 \times 10^{-3}$ . Our scheme also possesses fast long-range logical gates and low qubit overhead due to both its use of efficient topological error correction and its avoidance of state distillation.

The discussion is organized as follows. In Section II we review a 2-D color code from [18] which forms the error correction substrate of all that follows. Logical qubit initialization and measurement are described in Section III, with each logical qubit being represented by three defects. Section IV describes defect deformation. The basic logical gates CNOT,  $H$ ,  $X$ ,  $Z$  and  $S$  are detailed in Section V. Logical controlled- $TXT^\dagger$ , which enables the avoidance of state distillation, is discussed separately in Section VI. Section VII concludes and points to further work.

## II. ERROR CORRECTION SUBSTRATE

Consider Fig. 1. This shows a 2-D lattice of qubits arranged on faces with either 4 or 8 edges [18]. Each face is associated with two stabilizers [19]: the tensor product

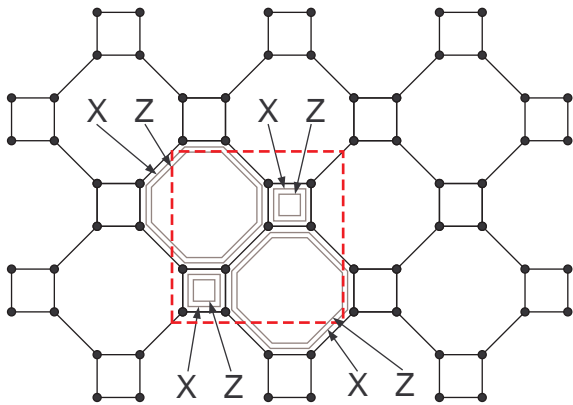


FIG. 1: The stabilizers of the error correction substrate. Dots indicate the location of qubits. The dashed box is a unit cell of the lattice containing 8 qubits and associated with 8 independent stabilizers.

of  $X$  on every qubit around the face and similarly for  $Z$ . Note that because every face has two qubits in common with its neighboring faces, all stabilizers commute. Note also that the unit cell indicated in Fig. 1 contains 8 qubits and can be associated with 8 independent stabilizers. An infinite lattice of this form therefore contains no logical qubits. In the absence of errors, the lattice of qubits is arranged to be in the simultaneous  $+1$  eigenstate of each stabilizer.

Fig. 2 contains examples of the effects of errors. Note that one of the three colors red, blue and green has been assigned to each of the faces such that no two adjacent faces have the same color. This will simplify the discussion of the various types of errors and the later discussion of logical operators. Every qubit is on three faces. If a qubit suffers an  $X/Z$  error, the  $Z/X$  stabilizers of these three faces become negative if no other error of the same type occurs on these three faces. A second error of the same type adjacent to the first error results in just two faces of the same color having negative stabilizers. Such chains of errors are said to have the same color as the faces they connect. A chain of each color can meet at a single qubit without changing the sign of any stabilizers. Arbitrarily complex error trees can occur with multiple intersections.

Additional syndrome qubits are required to determine the sign of the face stabilizers. For red faces, with just 4 data qubits, we choose to use just one additional syndrome qubit and the simple circuits shown in Fig. 3 to determine the sign of their associated  $X$  and  $Z$  stabilizers. Note that errors occurring during these circuits can propagate to the data qubits with a single syndrome qubit error propagating to multiple data qubits. For red faces, the potential number of effected data qubits is sufficiently low that we choose to leave the detection and correction of these errors to later rounds of syndrome extraction.

Green and blue faces, with 8 data qubits, could simply use the 8 qubit analogues of Fig. 3 and live with the fact that up to 4 data qubits could be effected by an error on the single syndrome qubit. We choose not to do this. Instead, 5 syndrome qubits are devoted to each green and blue face as shown in Fig. 4. Initially, the circuit of Fig. 5 is repeatedly executed until the central syndrome qubit is measured in state  $|0\rangle$  indicating successful preparation of a 4-qubit cat state provided no more than one error occurred during the execution of the circuit. The circuits of Fig. 6 and Fig. 7 are then executed for  $X$  and  $Z$  syndrome extraction respectively with each qubit of the cat state interacting with its two non-syndrome nearest neighbors.

In addition to reducing the number of data qubits that can be corrupted after a single error during syndrome extraction, a significant benefit of using 5 syndrome qubits on green and blue faces is avoiding the need to have a single syndrome qubit coupled to 8 data qubits, greatly simplifying the underlying lattice of qubits and network of connections. Note that in Fig. 4 no qubit is connected to more than 4 other qubits with most connected to just 3 other qubits. Note also that the concepts of color and the different face sizes arise only from how the underlying hardware is used, not from any aspect of its physical construction.

The rate at which a red syndrome extraction can be performed will be used as our unit of time. Note that green and blue syndrome extraction, being more complicated, will take more than one unit of time and, being nondeterministic, will take a variable amount of time. All syndrome changes are collected and stored in two 3-D data structures, one each for  $X$  and  $Z$  errors, an example of which is shown in Fig. 8. A single isolated syndrome measurement error is represented as two dots one above another — the first dot representing the incorrect measurement, different from the preceding correct measurement, and the second dot representing the following correct measurement, different from the preceding incorrect measurement.

The lattices we will discuss in this work will both have and make extensive use of boundaries. Fig. 9 shows examples of the three different colors of boundaries. At this point in the discussion, the only property of a boundary of a given color that is of interest is the fact that an error chain of the same color can connect to it without changing the sign of any stabilizers. An example of an error chain of each color starting at each boundary and meeting at a single qubit is shown.

In principle, after collecting a large amount of data, the minimum number of errors and the arrangement of these errors should be determined such that the observed syndrome information is reproduced. This arrangement of errors would then be applied manually to bring the surface back into the simultaneous  $+1$  eigenstate of every stabilizer. Given errors can occur in complicated trees as shown in Fig. 2, doing this exactly is unlikely to be computationally feasible. Instead, we use an approximate

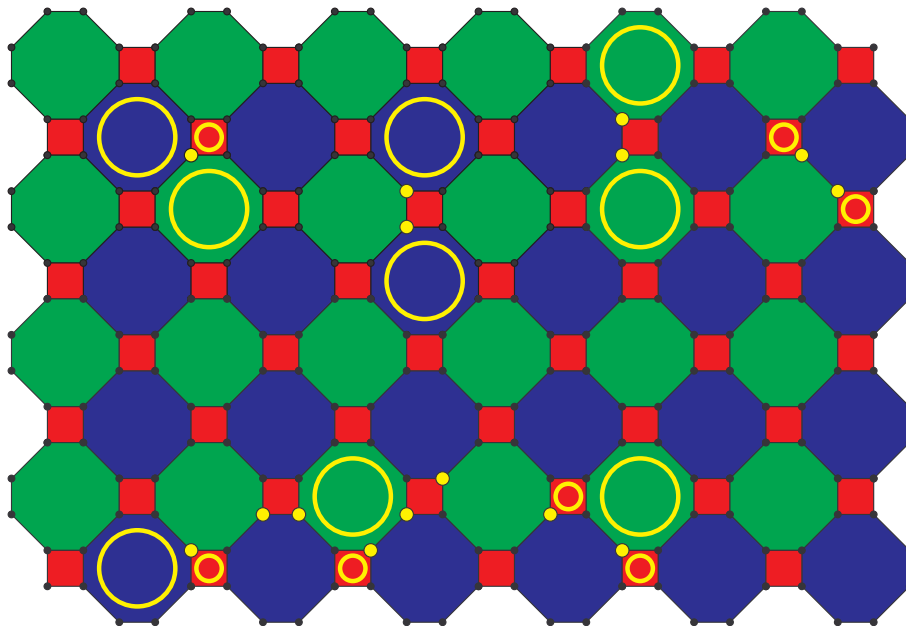


FIG. 2: Examples of errors in a color code (color online). Yellow dots indicate the locations of errors. Yellow circles indicate stabilizers of changed sign. As drawn, each chain of errors is of a single type  $X$  or  $Z$  and the neighboring stabilizers of changed sign are of type  $Z$  or  $X$ , respectively.

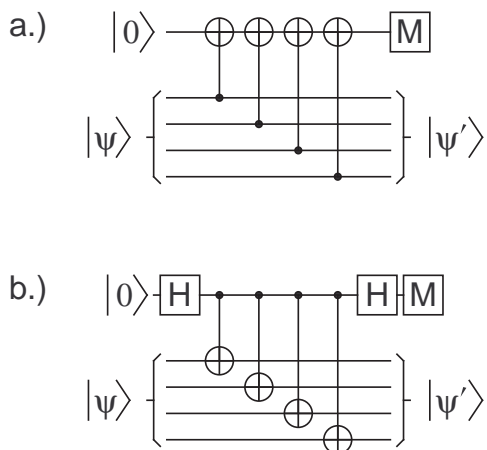


FIG. 3: Circuit showing how an additional syndrome qubit (top line of each figure) is used to measure red face a.)  $Z$  stabilizers, b.)  $X$  stabilizers.

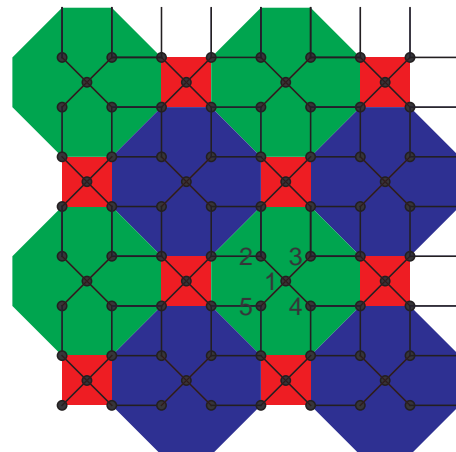


FIG. 4: Underlying lattice of physical qubits. Dots represent qubits, lines represent tunable interactions between qubits. The numbered qubits are used in Figs. 6–7.

approach based on three applications of the minimum weight matching algorithm [20], one for each color. The minimum weight matching algorithm takes a weighted graph as input and outputs a maximum length list of disjoint edges of minimum total weight.

Consider the red syndrome changes shown in Fig. 8. We will consider six ways of correcting the lattice given a red syndrome change: applying an appropriate chain of operators connecting the red syndrome change under consideration to another red syndrome change, a red

boundary, both a green and blue syndrome change, both a green and blue boundary, a green syndrome change and a blue boundary, and finally a green boundary and a blue syndrome change. Note that this is certainly not an exhaustive list of possibilities, merely a sufficiently inclusive list enabling the correction of arbitrary errors connected to red faces. To see that it is sufficiently inclusive, consider the situation not covered — a red syndrome change in a lattice with no other red syndrome changes, no red boundaries and all other syndrome changes and bound-

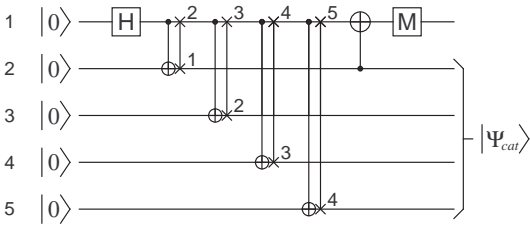


FIG. 5: Preparation of a 4-qubit cat state using the 5 qubits indicated in Fig. 4. The states initially stored in qubits 1–4 are manipulated to form a cat state stored on qubits 2–5. The state stored in qubit 5 is used to check the cat state and is read out using qubit 1.

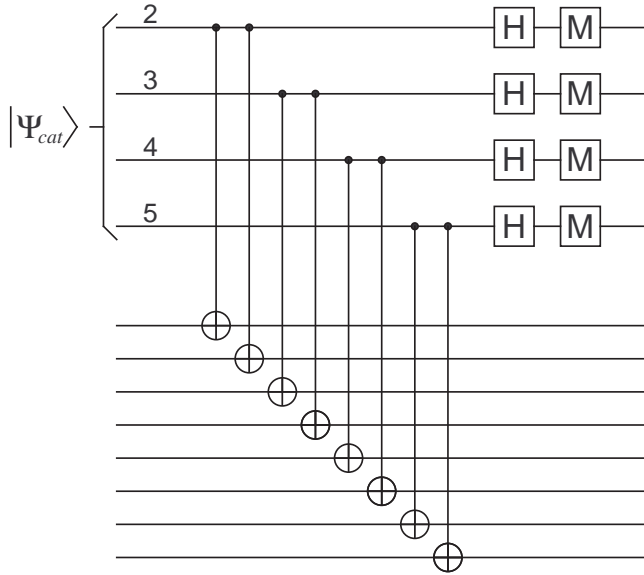


FIG. 6: Circuit used to determine the eigenvalue of the 8 qubit X stabilizer associated with a green or blue face.

aries of the same color. This situation can only arise as the result of incorrect syndrome measurement as if all syndrome measurements are correct the error chain beginning at the changed red syndrome must terminate either at another red face or branch and terminate at a collection of green and blue faces and boundaries. It is therefore acceptable to not attempt any correction of the solitary changed red syndrome and wait for further data to reveal the nature of the incorrect syndrome measurement.

As already stated above, the minimum weight matching algorithm takes a weighted graph as input. We start with a collection of abstract vertices corresponding to the red syndrome changes. A complete weighted graph is constructed on these vertices with weights corresponding to the sum of the number of time steps and minimum number of errors required to connect each pair of changes. Next, for each vertex, we determine the minimum length error chain, which may be branched, con-

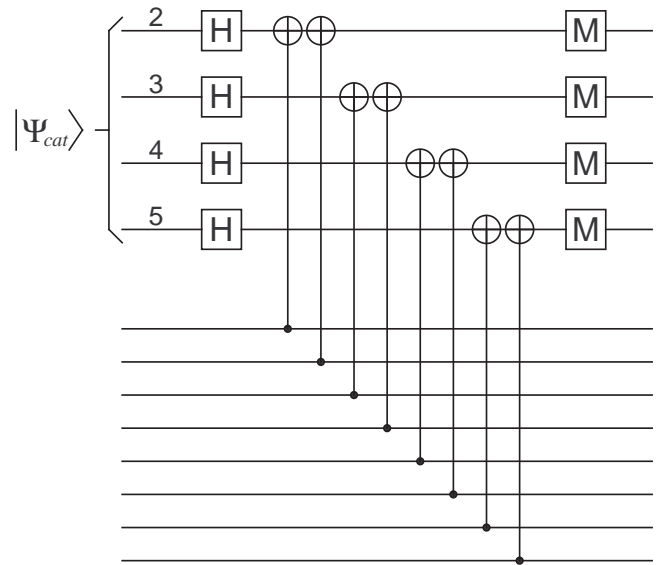


FIG. 7: Circuit used to determine the eigenvalue of the 8 qubit Z stabilizer associated with a green or blue face.

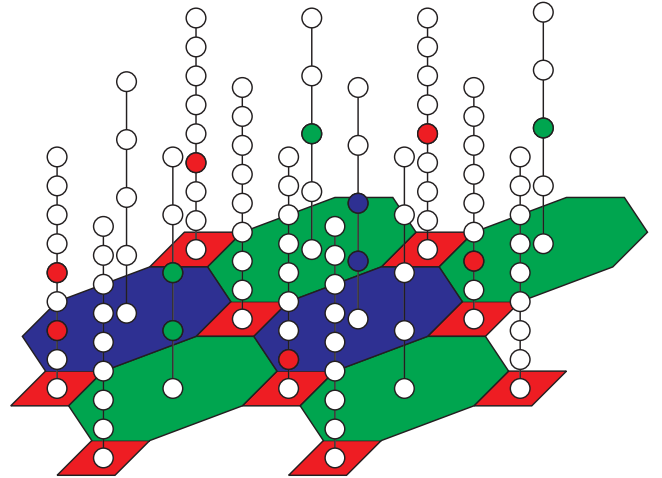


FIG. 8: Example of X or Z syndrome information.

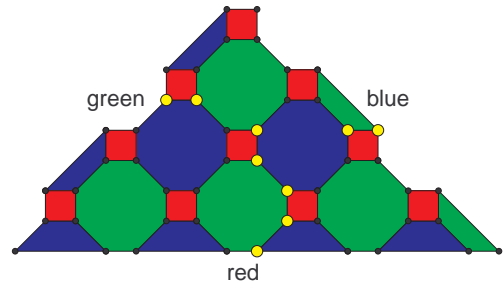


FIG. 9: Examples of the three colors of boundaries and error chains of each color starting at each boundary and meeting a single qubit.

necting the vertex to any allowed combination of boundaries and changed syndromes of different colors. Examples of each case we consider are shown in Fig. 10. This can be done efficiently as there are only a polynomial number of cases to check. For every existing vertex we add a second abstract vertex and connect them with an edge weighted with this minimum length. Finally, all of these secondary vertices are connected to one another with edges of weight zero. The minimum weight matching algorithm is then applied to this graph, and appropriate corrections applied according to the edges output. In practice, given a large number of time steps of data, corrections would not be applied to the very most recent time steps as syndrome information here has not had sufficient time to be verified by later measurements. The net effect of all of the above is to correct all red syndrome changes in a chosen region of space and time.

Correction continues by considering green and then blue syndrome changes in a very similar manner to red syndrome changes. The only difference is that since green and blue syndrome information is generated less frequently, weights in the time direction are reduced by a factor equal to the average amount of time required to perform a single syndrome extraction.

### III. LOGICAL QUBIT INITIALIZATION AND MEASUREMENT

In Section II we discussed an infinite lattice of qubits and a method of error correction, however the lattice contained no logical qubits. Logical qubits can be introduced by ceasing to enforce stabilizers and thereby introducing degrees of freedom into the lattice. We call a connected region of a single color of faces whose stabilizers we no longer enforce a defect. Examples of red, green and blue defects are shown in Fig. 11. Note that by connected we mean faces connected by an  $XX$  and a  $ZZ$  measurement. The effect of these measurements is to create a single large face of the same color as the constituent faces. Initially, provided the defect is constructed from the measurement of complete faces, it is in the  $+1$  eigenstate of its associated bounding  $X$  and  $Z$  stabilizers. We will henceforth always use defects constructed from the measurement of complete faces. Note that the bounding stabilizers can be regarded as rings of either of the two colors the defect isn't.

Before a defect can be used as part of a logical qubit, some of its neighboring stabilizers must be corrected. Stabilizers that have had their sides reduced by  $XX$  and  $ZZ$  measurements will have a sign dependent on the results of these measurements. Note that such reduced size stabilizers of negative sign always occur in pairs. They can therefore also be connected and corrected in pairs using appropriate chains of operators.

Note that direct  $XX$  and  $ZZ$  measurements are actually not necessary to create a large defect. It is equivalent and simpler to just measure the stabilizers of reduced

size. The qubits inside the defect can be ignored. These inner qubits only become important again if the size of the defect is reduced.

Many types of logical qubits are possible. We will be interested in logical qubits consisting of three defects, one of each color. Note that chains of operators of the same color commute regardless of whether they consist of  $X$  or  $Z$  operators as they always have an even number of qubits in common. Fig. 12 shows examples of the two types of triple defect logical qubits we will use. We call logical qubits with triangular  $X_L$  operators “primal” and those with triangular  $Z_L$  operators “dual”. Primal qubits will store the data in our computer whereas dual qubits will facilitate multiple qubit gates. Note that the six types of primal  $Z_L$  operators are equivalent in the sense that they all commute with one another and all anticommute with primal  $X_L$ . When performing a logical phase-flip, it does not matter which primal  $Z_L$  operator is used. Dual  $X_L$  operators are also all equivalent.

Primal qubits are naturally initialized to the  $+1$  eigenstate of  $Z_L$ , namely  $|0_L\rangle$ . Similarly, dual qubits are naturally initialized to  $|+_L\rangle$ . Note that since primal and dual qubits are structurally identical, when we create a logical qubit we actually create both a primal and a dual qubit. Furthermore, we do nothing to distinguish these two types of qubits. As we shall see, computation proceeds with both types of qubit present and we simply ignore one type and focus on the computation occurring in the qubit type of interest.

Measurement of a logical qubit can be performed transversely by measuring a region of qubits encompassing the three defects in either the  $X$  or  $Z$  basis. Measurement results are error corrected using the standard algorithm with syndromes calculated from the parity of measurement results around each face. After error correction, provided no logical errors have occurred, all rings of measurements around each defect will have the same parity and similarly all three-way chains of measurements connecting all three defects will have the same parity. These parities are the logical measurement results. Note that when performing the transversal  $X/Z$  measurements we perform both a primal and a dual  $X_L/Z_L$  measurement. The unnecessary logical measurement result is simply ignored.

Primal/dual qubits can also be initialized to  $|+_L\rangle/|0_L\rangle$  by first initializing a region of qubits to  $|+\rangle/|0\rangle$  and then creating defects by measuring appropriate  $Z/X$  stabilizers. These stabilizers will have random sign initially, and must be corrected before the logical qubit is used.

A number of different types of logical errors are possible. Fig. 13 contains a few examples. If an error chain half encircles a defect, it cannot be reliably corrected as given only endpoint information is not possible to know which half of the defect is encircled and thus which half of the defect to apply corrective operations to. If the wrong half is chosen, we form a logical operation instead of correcting the error. For primal/dual qubits, half rings of  $Z/X$  errors are dangerous. Similarly, if a collection of dif-

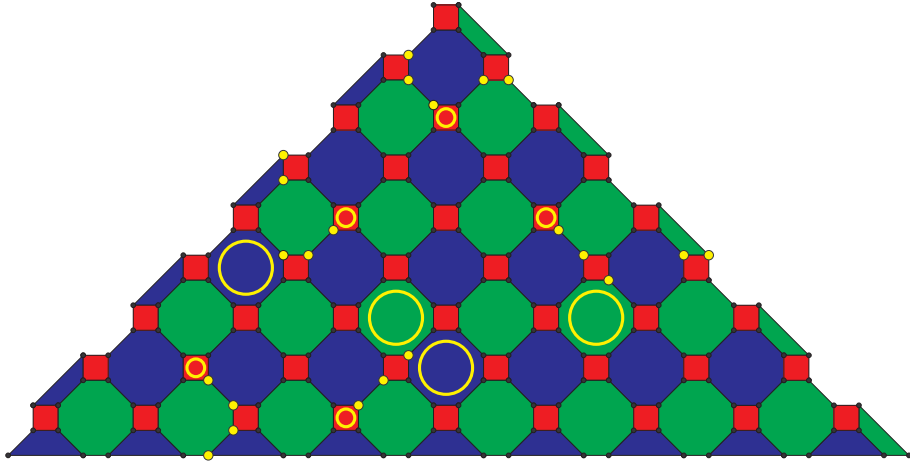


FIG. 10: Examples of the five methods of correcting a red syndrome change we consider in addition to connecting it to another red syndrome change. Left to right, top to bottom, these examples show a red syndrome change connected to a green and blue boundary, a green boundary and blue face, a green face and blue boundary, a red boundary, and a green and blue face.

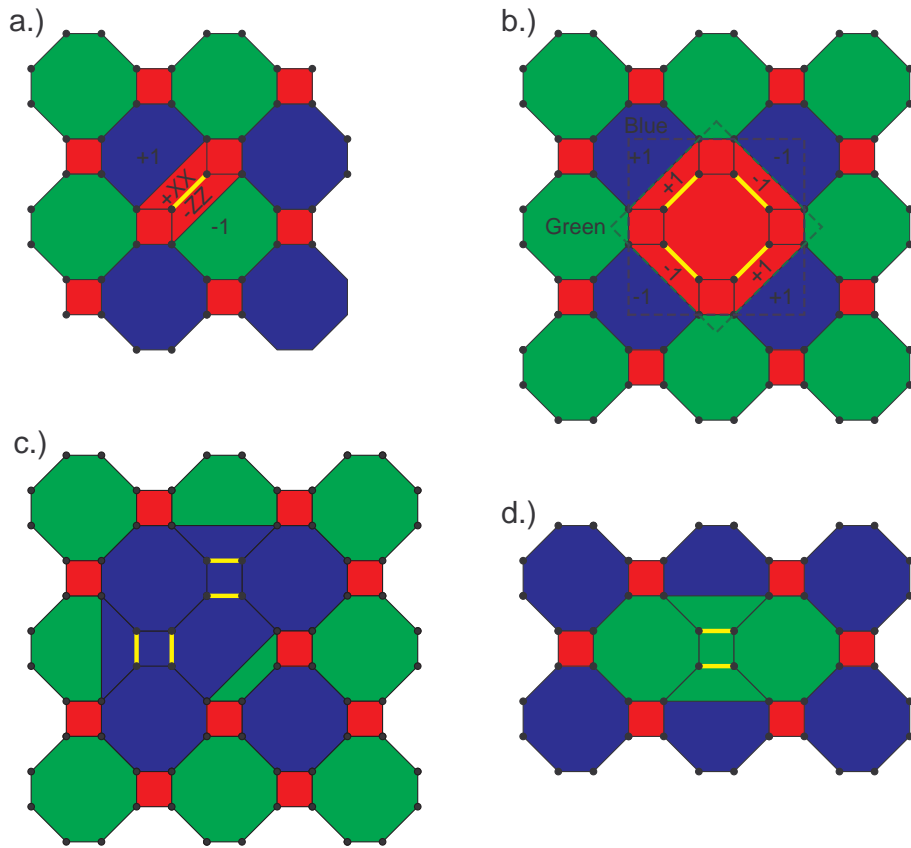


FIG. 11: a.) Red defect created by measuring  $XX$  and  $ZZ$  on the qubits indicated by a yellow line (color online). The signs of these measurements determine the signs of the stabilizers of the neighboring faces of reduced size. b.) Red defect created by measuring a complete face. Equivalent blue and green boundary stabilizers with positive sign independent of the measurement results assuming no errors. These boundary stabilizers are always positive as they are equal to the product of the five complete face stabilizers contained within the effect. c.) Blue defect. d.) Green defect.

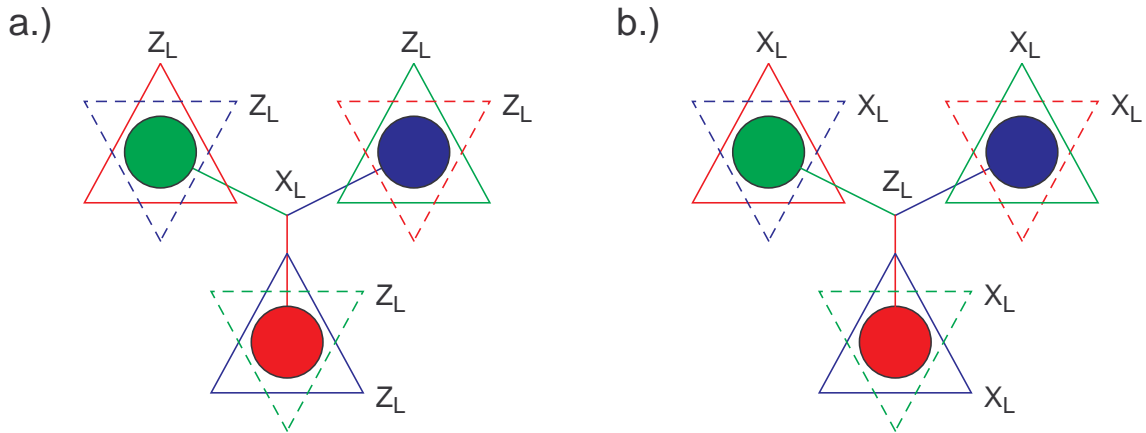


FIG. 12: A defect of each color forming a.) a primal qubit, b.) a dual qubit. Note that the six primal  $Z_L$  and dual  $X_L$  operators are equivalent.

ferent color error chains half constructs a three-way connection, the error correction procedure cannot in general determine which half has been constructed and correct it. For primal/dual qubits, half connections of  $X/Z$  errors are dangerous. Furthermore, individual defects of a given color can be half connected to other defects of the same color by error chains or half connected to boundaries of the same color. Both situations correspond to errors that cannot be reliably corrected. Given the rich error structure of color codes, an unlimited number of additional types of logical errors are possible, though suppressed if boundaries and defects are kept well separated. Note that the strength of  $X/Z$  error correction can be independently set by adjusting the circumference and separation of defects.

#### IV. DEFECT DEFORMATION

We have discussed error correction and the creation and measurement of logical qubits. We now turn our attention to the techniques required to perform computation. Defect expansion and contraction can be used to adjust the size of a defect and thus the local error correction strength. By combining expansion and contraction, defects can be moved and braided around one another, realizing multiple qubit gates as we shall see in Sections V–VI. Expanding all three defects comprising a logical qubit until they touch and creating an enclosed triangular region isolates the logical qubit from the rest of the lattice, enabling transversal gates to be applied.

Consider Fig. 14a. This shows the procedure for expanding a red defect and the effect of doing so on both a green and blue stabilizer. Fig. 14b shows the effect of contracting a defect on a red stabilizer attached to the defect. Note that even in the absence of errors, corrective operations must be applied when moving the defect to ensure that the signs of all stabilizers remain unchanged at

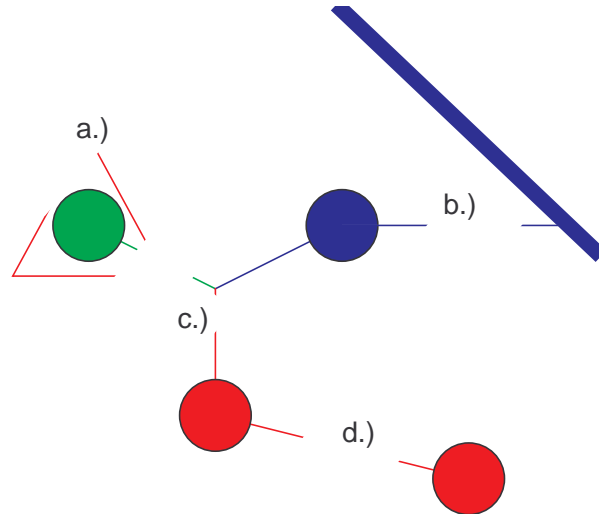


FIG. 13: Examples of error chains likely to lead to logical errors. a.) Half encircling a defect. b.) Half connecting a defect to a boundary of the same color. c.) Half connecting the three defects. d.) Half connecting a defect to another of the same color.

the end of the procedure. The procedures for expanding and contracting green and blue defects are analogous.

Fig. 15 shows the effect of isolating a triangular region of the lattice, the detailed structure of which can be found in Figs. 9–10, by simultaneously expanding all three defects comprising a logical qubit. Stabilizers encircling a defect are converted into pairs of three-way stabilizers. Sections V and VI both make use of such isolated regions. Note that the isolation is reversible by simply contracting the defects once more.

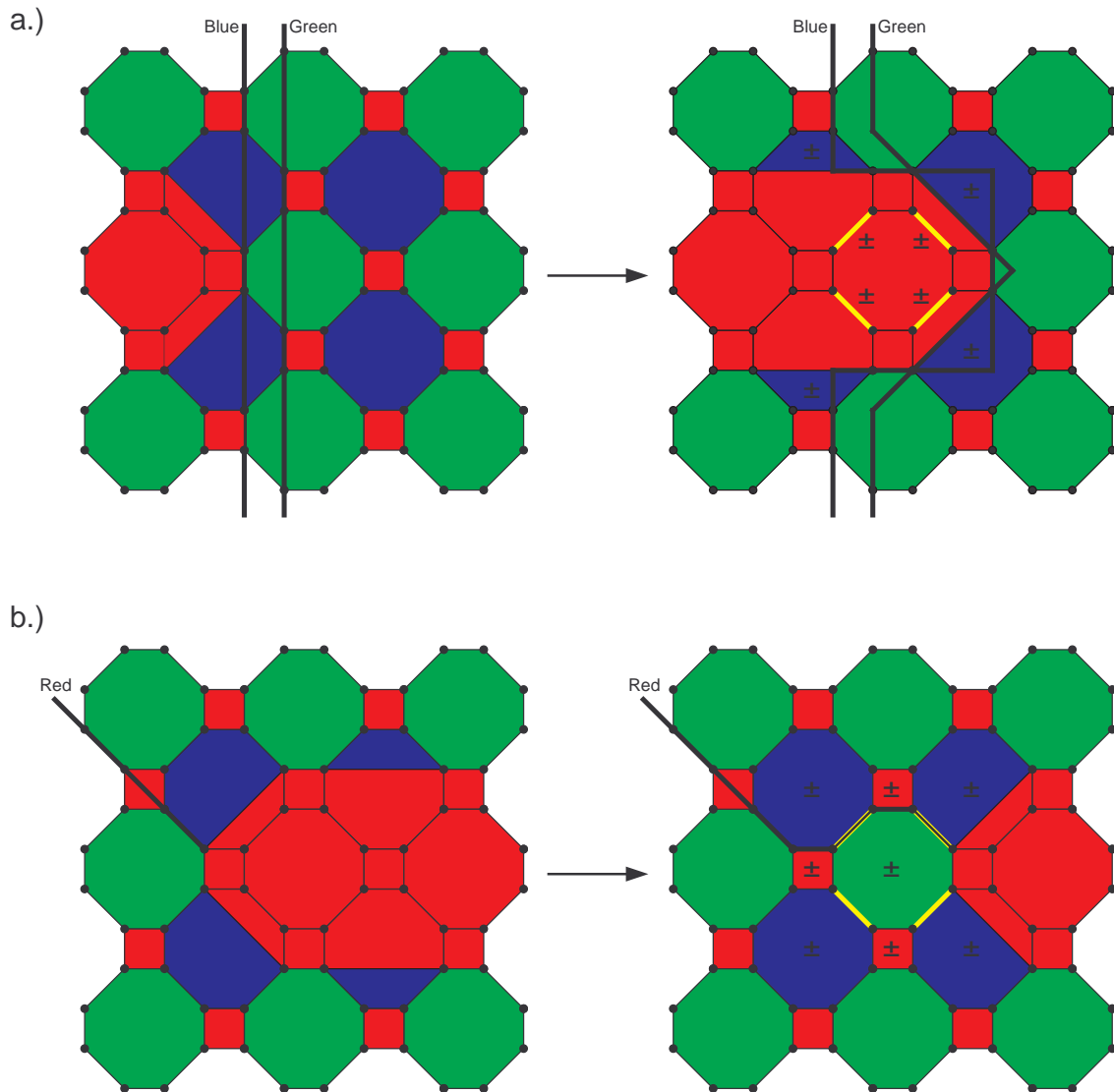


FIG. 14: a.) Procedure for expanding a red defect. It is conceptually simpler to imagine that the operators  $XX$  and  $ZZ$  are measured directly on the qubits on the yellow lines (color online), but in practice these qubits can be ignored and only the stabilizers of the indicated partial faces measured. b.) Procedure for contracting a red defect. The full stabilizers of the indicated faces are measured once more. The signs of these face stabilizers are then corrected using the regular error correction procedure.

## V. BASIC LOGICAL GATES

In this section, we describe the logical gates CNOT,  $H$ ,  $X$ ,  $Z$  and  $S$ . By far the simplest logical gates are  $X_L$  and  $Z_L$ , which can be implemented with simple rings and three-way trees of single-qubit operators. We shall not discuss these further. The remaining logical gates require individual discussion.

Logical Hadamard,  $H_L$ , shall be applied transversely to an isolated triangular logical qubit, however some care is required. Given a primal/dual qubit, during the isolation process  $Z_L/X_L$  is split into two three-way trees. The tree external to the isolated region must be removed before

transversal gates can be applied. This can be achieved by measuring a region of qubits around the isolated region in the  $Z/X$  basis. Note that all external operator trees must have the same parity in the absence of errors and that the standard error correction procedure can be used to ensure that the parity is determined fault-tolerantly. Note that this does not constitute logical measurement of  $Z_L/X_L$  as the isolated region is not measured and the parity of internal three-way trees must also be known to effect logical measurement. Measuring the parity  $s$  of external trees does, however, introduce a byproduct operator  $X_L^s/Z_L^s$ . With the external trees pruned, logical Hadamard can then be applied transversely. The

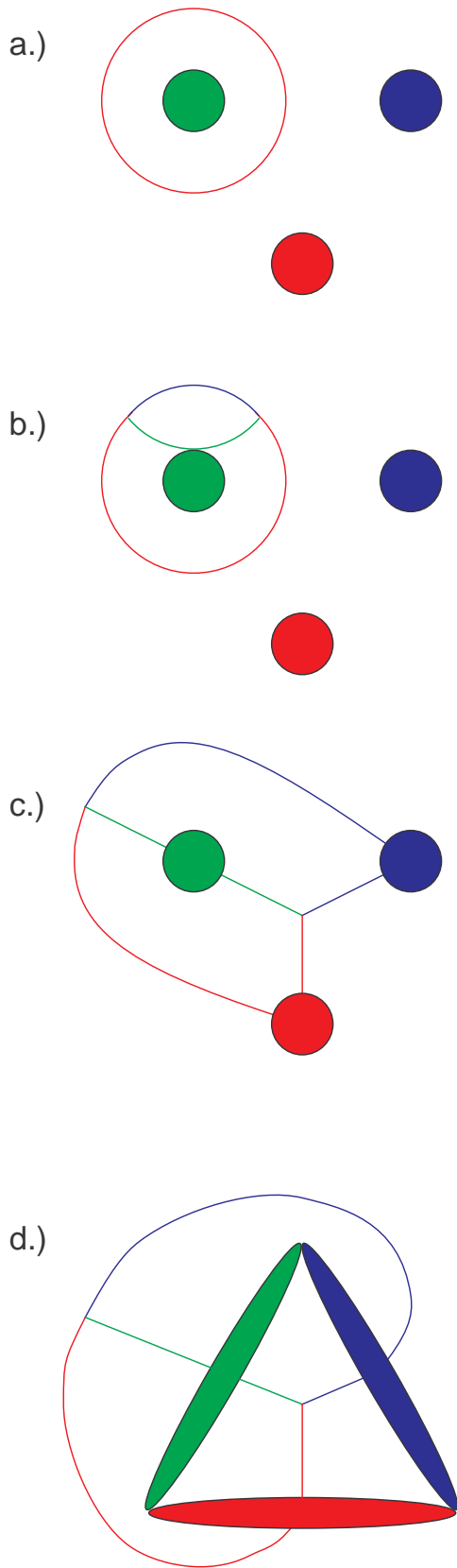


FIG. 15: Step-by-step deformation of a ring operator into a pair of tree operators via deformation of the associated defects to create an isolated region of lattice.

appropriate external face stabilizers must be measured and corrected before the logical qubit is converted back to three isolated defects. The conversion back can also introduce a byproduct operator.

Logical  $S$  requires a different type of care. In this case, the external trees do not need to be pruned, however we need to ensure that the correct number of qubits have been enclosed. In the original color code work, triangular logical qubits with  $3 \bmod 4$  total physical qubits and either 4 or 8 qubits per face were used [18]. For convenience, we require there to be  $1 \bmod 4$  enclosed qubits. Using enclosed regions of the form shown in Figs. 9–10, this can be achieved by having an even number of rows of red faces. When single-qubit  $S$  is applied transversely, the condition of having either 4 or 8 qubits per face ensures that every state comprising  $|0_L\rangle$  and every state comprising  $|1_L\rangle$  acquires the same phase. Having  $1 \bmod 4$  qubits in total ensures that  $|0_L\rangle \mapsto |0_L\rangle$  and  $|1_L\rangle \mapsto i|1_L\rangle$ . Transversal  $S$  thus implements  $S_L$ .

With an odd number of enclosed qubits and every three-way chain containing an odd number of operators, we can also implement  $X_L$  and  $Z_L$  transversely. While this would not be done under normal circumstances, as it is easier to simply apply ring or tree operators to non-isolated logical qubits, if the logical qubit has already been isolated, the ability to apply transversal  $X_L$  and  $Z_L$  enables us to avoid further modification of the shape of the logical qubit.

Logical CNOT is carried out in a similar manner to the schemes of [2, 4]. A primal qubit can be used to control a CNOT gate with a dual qubit as target as shown in Fig. 16. Note that all of the CNOT stabilizer mappings  $XI \mapsto XX$ ,  $IX \mapsto IX$ ,  $ZI \mapsto ZI$  and  $IZ \mapsto ZZ$  are faithfully realized. We can then use the circuit shown in Fig. 17 to simulate CNOT between two primal qubits.

## VI. LOGICAL CONTROLLED- $TXT^\dagger$

We have described two types of qubits and how to initialize these qubits to  $|0_L\rangle$  and  $|1_L\rangle$ , measure them in the  $Z_L$  and  $X_L$  bases and perform logical gates CNOT,  $H$ ,  $X$ ,  $Z$  and  $S$ . This is not sufficient for universal quantum computation. To achieve universality, we construct logical controlled- $TXT^\dagger$ , where

$$T = \begin{pmatrix} 1 & 0 \\ 0 & e^{i\pi/4} \end{pmatrix} \quad (1)$$

With this gate, we can build the circuit of Fig. 18, which deterministically and fault-tolerantly implements the single logical qubit rotation  $T$ . Preparation of  $|0_L\rangle$  together with logical CNOT,  $H$  and  $T$  and logical  $Z$  measurement is sufficient for universal quantum computation [21]. The additional logical gates in our toolbox make computation more efficient.

The sequence of gates  $T^\dagger$  (on the target qubit), CNOT,  $T$  is equivalent to controlled- $TXT^\dagger$ . If the control qubit is  $|0\rangle$ ,  $TT^\dagger = I$  is applied to the target qubit, if  $|1\rangle$ ,  $TXT^\dagger$

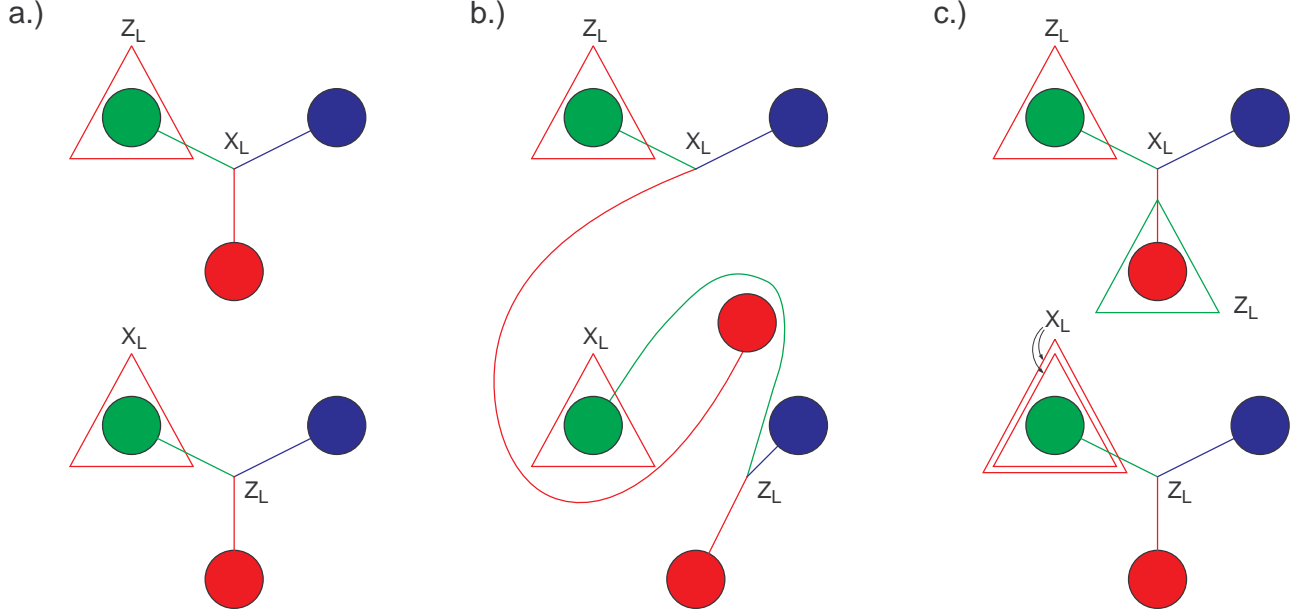


FIG. 16: Logical CNOT via braiding with a primal qubit (top) as control and dual qubit (bottom) as target. The appropriate mappings of logical stabilizers  $XI \mapsto XX$ ,  $IX \mapsto IX$ ,  $ZI \mapsto ZI$  and  $IZ \mapsto ZZ$  can be seen by tracing the deformation of one logical stabilizer at a time.

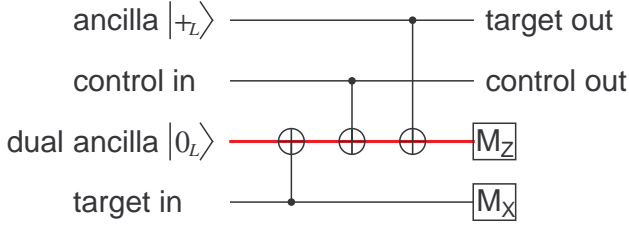


FIG. 17: Circuit constructed from available components implementing primal-primal logical qubit CNOT.

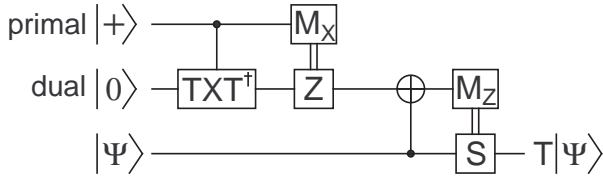


FIG. 18: Circuit constructed from available components implementing the single logical qubit rotation  $T$

is applied. While we cannot implement logical  $T$  transversely, logical  $TXT^\dagger = e^{-i\pi/4}SX$  is a transversal gate on enclosed logical qubits as described in the previous section. To complete the proof that logical controlled- $TXT^\dagger$  is possible in our scheme, we need to show that it is possible to perform a controlled bit-flip of an enclosed logical qubit using only defect deformation.

Firstly, note that it is possible to unenclose and re-enclose a logical qubit without disturbing its state. The logical operators are simply deformed and then returned to their original shape. We could therefore start with two enclosed logical qubits, unenclose them both, perform logical CNOT via braiding and then re-enclose them both. Since  $X_L$  is transversal on enclosed qubits, the above procedure would implement the desired controlled bit-flip. In our case we will not need to enclose the control qubit.

While the above discussion is sufficient to show that logical controlled- $TXT^\dagger$  is possible, we must also show that it is fault-tolerant. Consider Fig. 19. This shows the complete procedure for fault-tolerant logical controlled- $TXT^\dagger$ . Note that for simplicity the braided CNOT has been shown as being performed outside the region modified by  $T^\dagger$ . The face stabilizers in this region are now comprised of  $Z$  and  $T^\dagger XT$  operators. Note that these operators are orthogonal and anticommute and as such error correction can proceed in this region despite the fact we have technically left the code space of the color code. Furthermore, we do not, in fact, need to avoid braiding through this region. To extend and contract defects in this region one simply needs to measure qubits in the  $Z$  and  $T^\dagger XT$  bases.

## VII. CONCLUSION

We have described how to perform universal fault-tolerant quantum computation without state distilla-

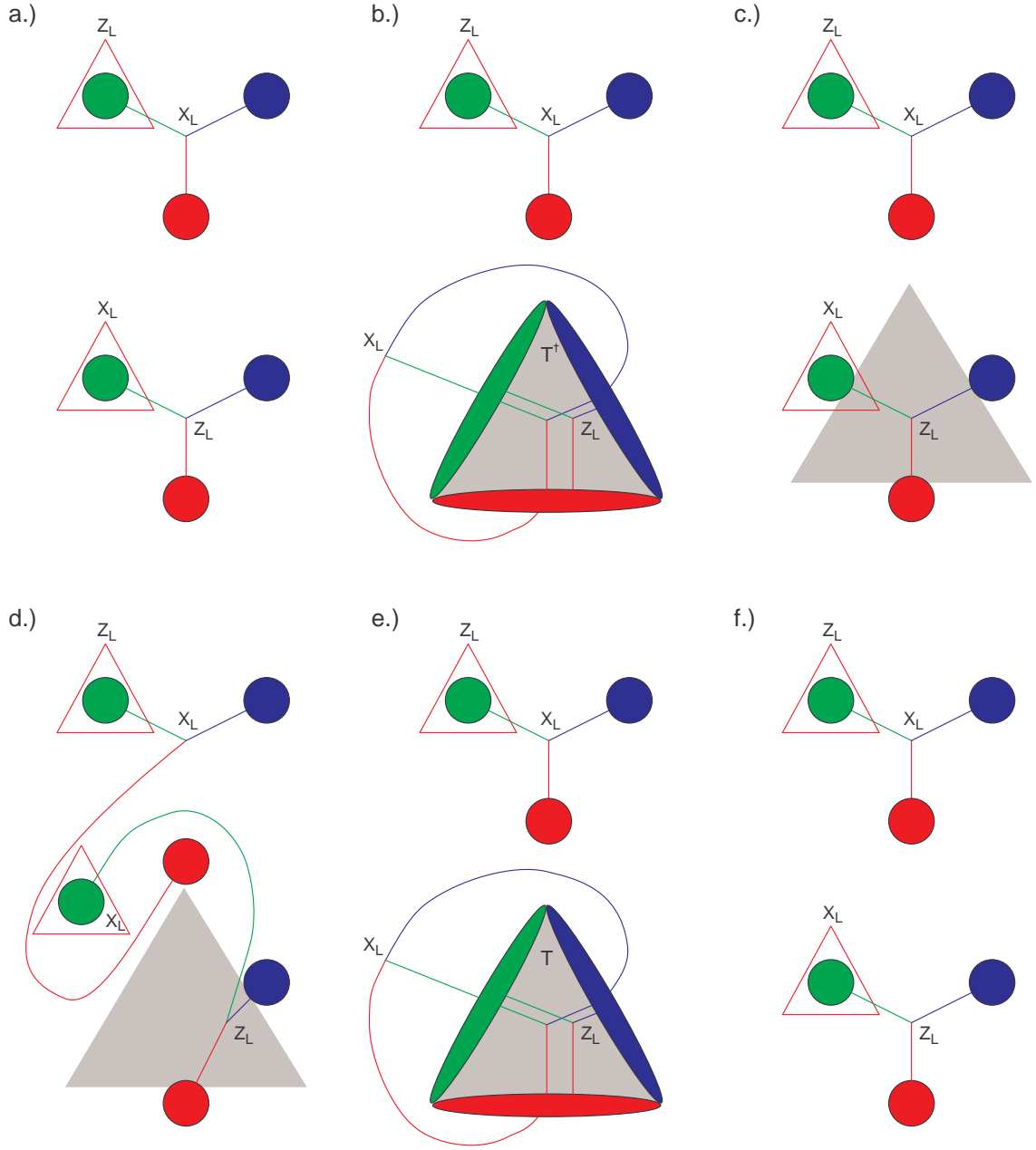


FIG. 19: Procedure for performing tolerant logical controlled- $TXT^\dagger$ . As this is not a Clifford group gate and we leave the code space during the operation, the mapping of stabilizers cannot readily be shown and therefore has not been shown. The indicated logical operators should only be considered a rough guide to what is happening in each step. a.) Primal control qubit (top), dual target qubit (bottom). b.) Enclose target qubit and apply transversal  $T^\dagger$  to the shaded triangular isolated region. c.) Unenclose target qubit and continue error correction in changed basis. d.) Braided logical CNOT. e.) Enclose target qubit and apply transversal  $T$  to the shaded triangular isolated region. This returns us to the code space. f.) Unenclose target qubit.

tion on a specific 2-D color code. This scheme has a high threshold, low overhead, adjustable asymmetric error correction, fast long-range logical gates and makes few demands on the underlying hardware. Our scheme calls for a measurement time of the same order as the gate times, local single qubit unitaries and a 2-D nearest neighbor tunably coupled lattice of qubits, with each

qubit coupled to either 3 or 4 neighbors and with no couplings crossing. This lattice is shown in Fig. 4. Ideally, it should be possible to simultaneously measure an arbitrary subset of qubits in the lattice, although if measurement hardware cannot be located near every qubit, it would be sufficient to be able to measure a fraction of the qubits that is independent of the lattice size.

As described, our scheme brings together all of the desirable properties of error correction and fault-tolerant quantum computation. As such, it represents a major advance over prior schemes. We believe the scheme has a good chance of one day being used in a practical large-scale quantum computer.

Further work is required to determine the precise threshold error rate. It is expected to lie between  $10^{-3}$

and  $10^{-2}$  given the similarity of the underlying error correction to schemes for which the threshold error rate has been calculated. An important open question is whether it is possible to modify the scheme so that only a 1-D chain or a narrow 1-D stripe of qubits is required, eliminating the significant engineering challenges arising from the requirement of a 2-D lattice.

- 
- [1] R. Raussendorf and J. Harrington, Phys. Rev. Lett. **98**, 190504 (2007), quant-ph/0610082.
  - [2] R. Raussendorf, J. Harrington, and K. Goyal, New J. Phys. **9**, 199 (2007), quant-ph/0703143.
  - [3] H. Bombin and M. A. Martin-Delgado, arXiv:0704.2540v1 (2007).
  - [4] A. G. Fowler, A. M. Stephens, and P. Groszkowski, arXiv:0803.0272 (2008).
  - [5] A. G. Fowler and K. Goyal, arXiv:0805.3202 (2008).
  - [6] R. P. Feynman, Int. J. Theor. Phys. **21**, 467 (1982).
  - [7] D. Deutsch and R. Jozsa, Proc. R. Soc. Lond. A **439**, 553 (1992).
  - [8] P. W. Shor, in *Proc. 35th Annual Symposium on Foundations of Computer Science* (1994), pp. 124–134.
  - [9] A. Y. Kitaev, Tech. Rep. TR96-003, Electronic Colloquium on Computational Complexity (1996), quant-ph/9511026.
  - [10] L. K. Grover, in *Proc. Twenty-Eighth Annual ACM Symposium on the Theory of Computing* (1996), pp. 212–219, quant-ph/9605043.
  - [11] V. Subramaniam and P. Ramadevi, quant-ph/0210095 (2002).
  - [12] P. W. Shor, Phys. Rev. A **52**, R2493 (1995).
  - [13] A. R. Calderbank and P. W. Shor, Phys. Rev. A **54**, 1098 (1996), quant-ph/9512032.
  - [14] A. M. Steane, Proc. R. Soc. Lond. A **425**, 2551 (1996), quant-ph/9601029.
  - [15] S. Bravyi and A. Kitaev, Phys. Rev. A **71**, 022316 (2005), quant-ph/0403025.
  - [16] B. W. Reichardt, Quant. Info. Proc. **4**, 251 (2005), quant-ph/0411036.
  - [17] M. A. Nielsen and I. L. Chuang, *Quantum Computation and Quantum Information* (Cambridge University Press, Cambridge, 2000).
  - [18] H. Bombin and M. A. Martin-Delgado, Phys. Rev. Lett. **97**, 180501 (2006), quant-ph/0605138.
  - [19] D. Gottesman, Ph.D. thesis, Caltech (1997), quant-ph/9705052.
  - [20] W. Cook and A. Rohe, INFORMS J. Comput. **11**, 138 (1999).
  - [21] P. O. Boykin, T. Mor, M. Pulver, V. Roychowdhury, and F. Vatan, Inform. Process. Lett. **75**, 101 (2000).